ACCOUNTS of chemical research

Article

pubs.acs.org/accounts

Electron Injection Dynamics in High-Potential Porphyrin Photoanodes

Published as part of the Accounts of Chemical Research special issue "Ultrafast Excited-State Processes in Inorganic Systems".

Rebecca L. Milot[†] and Charles A. Schmuttenmaer*

Department of Chemistry and Energy Sciences Institute, Yale University, 225 Prospect Street, P.O. Box 208107, New Haven, Connecticut 06520-8107, United States

CONSPECTUS: There is a growing need to utilize carbon neutral energy sources, and it is well known that solar energy can easily satisfy all of humanity's requirements. In order to make solar energy a viable alternative to fossil fuels, the problem of intermittency must be solved. Batteries and supercapacitors are an area of active research, but they currently have relatively low energy-to-mass storage capacity. An alternative and very promising possibility is to store energy in chemical bonds, or make a solar fuel.

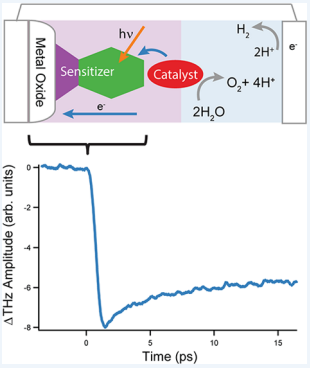

The process of making solar fuel is not new, since photosynthesis has been occurring on earth for about 3 billion years. In order to produce any fuel, protons and electrons must be harvested from a species in its oxidized form. Photosynthesis uses the only viable source of electrons and protons on the scale needed for global energy demands: water. Because artificial photosynthesis is a lofty goal, water oxidation, which is a crucial step in the process, has been the initial focus. This Account provides an overview of how terahertz spectroscopy is used to study electron injection, highlights trends from previously published reports, and concludes with a future outlook. It begins by exploring similarities and differences between dye-sensitized solar cells (DSSCs) for producing electricity and a putative device for splitting water and producing a solar fuel. It then identifies two important problems encountered when adapting DSSC technology to water oxidation—improper energy matching between sensitizer energy levels with the potential for water oxidation and the instability of common anchoring groups in water—and discusses steps to address them. Emphasis is placed on electron injection from sensitizers to metal oxides because this process is the initial step in charge transport. Both the rate and efficiency of electron injection are analyzed on a sub-picosecond time scale using time-resolved terahertz spectroscopy (TRTS).

Bio-inspired pentafluorophenyl porphyrins are promising sensitizers because their high reduction potentials are compatible with the energy requirements of water oxidation. TRTS of free-base and metalated pentafluorophenyl porphyrins reveal inefficient electron injection into TiO_2 nanoparticles but more efficient electron injection into SnO_2 nanoparticles. With SnO_2, injection time scales depend strongly on the identity of the central substituent and are affected by competition with excited-state deactivation processes. Heavy or paramagnetic metal ions increase the electron injection time scale by roughly one order of magnitude relative to free-base or Zn^{2+} porphyrins due to the possibility of electron injection from longer-lived, lower-lying triplet states. Furthermore, electron injection efficiency loosely correlates with DSSC performance.

The carboxylate anchoring group is commonly used to bind DSSC sensitizers to metal oxide surfaces but typically is not stable under the aqueous and oxidative conditions required for water oxidation. Electron injection efficiency of several water-stable alternatives, including phosphonic acid, hydroxamic acid, acetylacetone, and boronic acid, were evaluated using TRTS, and hydroxamate was found to perform as well as the carboxylate.

The next challenge is incorporating a water oxidation catalyst into the design. An early example, in which an Ir-based precatalyst is cosensitized with a fluorinated porphyrin, reveals decreased electron injection efficiency despite an increase in photocurrent. Future research will seek to better understand and address these difficulties.

INTRODUCTION

Concerns about increasing global energy demands and the detrimental effects of continued use of fossil fuels have encouraged the investigation of solar energy as a renewable alternative. Among the many solutions, dye-sensitized solar cells (DSSCs) are a promising low cost option using earth-abundant materials.[1,2] In a typical DSSC (Figure 1A), a thin film of metal oxide nanoparticles, usually TiO_2, is deposited on a glass substrate coated with a transparent conducting oxide layer (TCO). Because TiO_2 is a wide band gap semiconductor, the nanoparticles are sensitized with a dye molecule, which absorbs photons over a large portion of the visible spectrum. The resulting photoanode is immersed in an electrolyte

Received: October 2, 2014
Published: May 4, 2015

DOI: 10.1021/ar500363q
Acc. Chem. Res. 2015, 48, 1423−1431

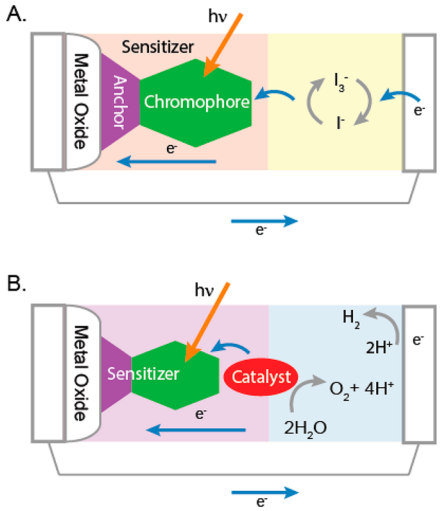

Figure 1. Schematic diagrams highlighting the basic operational principles of a DSSC (A) and an analogous device for water oxidation (B).

solution containing a redox couple, and a second TCO-coated glass substrate coated with a catalytic platinum film serves as the counter electrode. Upon light absorption by the sensitizer, an electron is transferred from its excited state to the metal oxide conduction band. The neutral ground state of the sensitizer is regenerated via oxidation of I^- to I_3^- in the electrolyte solution. The photoinjected electrons diffuse through the nanoparticle thin film until they collect at the TCO electrode, at which point they are transported through an external circuit to the counter electrode. Finally, I_3^- is reduced to I^- at the counter electrode so that the process may begin again.

Conversion of sunlight to electricity has inherent limitations, however, because solar energy is both diffuse and intermittent. Furthermore, electricity is difficult to store efficiently and transport over long distances, despite the progress being made with batteries, capacitors, and high-temperature superconducting cables.[3] Methods for converting sunlight into chemical fuels, which can be easily stored and transported, provide an ideal solution to these problems. Nature captures and stores solar energy through the process of photosynthesis. The water oxidation half reaction, a key step in photosynthesis in which water is converted to protons and electrons for fuel formation (with oxygen as a byproduct), has been the basis of many artificial photosynthesis strategies.[4]

$$2H_2O \rightarrow O_2 + 4H^+ + 4e^-$$

One strategy for photoelectrochemical water oxidation uses the principles of DSSCs,[5,6] and Figure 1B compares such a device to the DSSC depicted in Figure 1A. As in a DSSC, light absorption and charge collection are accomplished using a dye-sensitized metal oxide electrode. The dye ground state is regenerated through the oxidation of water rather than the redox couple. The "redox couple" (i.e., water) is not itself regenerated as in a DSSC, since the protons and electrons are used to produce fuels such as hydrogen or methanol. Because water oxidation is kinetically and thermodynamically demanding, a water oxidation catalyst must be included in the design, although the method for coupling the catalyst to the other components of the system has not been standardized.[5,7]

Despite the promise of these systems, efficiencies remain low, and few have detected measurable oxygen evolution even with an applied bias voltage.[5] One explanation for the low efficiencies of these devices is that well-established DSSC paradigms cannot be applied directly to water oxidation. A fundamental difference is that photochemical water oxidation is a four photon, four electron process and is therefore slow compared with the I^-/I_3^- reaction. As a result, losses due to recombination with the sensitizer cation are more likely.[8] In addition, the redox potential for water oxidation is more positive (lower in energy) than that for I^-/I_3^-, which precludes using the same sensitizers. Furthermore, most of the sensitizers designed for DSSCs are anchored to the metal oxide surface with carboxylate groups, which can undergo hydrolysis under aqueous conditions.[7,9]

At Yale, we are working to address all of these problems and have made significant progress addressing the issues of redox potential and water-stable anchoring groups. In addition to designing better sensitizers, we have also sought to understand the underlying physical processes involved in these systems in order to better inform future design modifications. Our approach in the Schmuttenmaer group has been to focus initially on electron injection.

In the context of both DSSCs and water oxidation, efficient electron injection is essential to the overall process because it initiates charge transport within the system. Because it occurs on a femtosecond to picosecond time scale, many ultrafast spectroscopic methods, including visible transient absorption spectroscopy and terahertz spectroscopy, have been used to analyze the process.[8]

This Account describes electron injection from high-potential porphyrin sensitizers designed for water oxidation and also analyzes the electron injection efficiency of several water-stable anchoring groups. It provides an overview of how terahertz spectroscopy is used to study electron injection, highlights trends from several previously published reports,[10−14] and concludes with a future outlook.

TERAHERTZ SPECTROSCOPY

Terahertz spectroscopy, which is distinguished from other far-infrared and millimeter wave spectroscopies by its sub-picosecond time resolution, is a versatile technique that has been used to study many phenomena including low-frequency vibrational modes in crystals,[15] solvation dynamics of proteins,[16] and photoinduced charge transfer from dyes.[17]

Time-resolved terahertz spectroscopy (TRTS) is an optical pump/terahertz probe technique used to measure the time- and frequency-dependent photoconductivity of bulk and nanocrystalline semiconductors in a noncontact fashion.[8,18−22] Because mobile electrons decrease the transmission of terahertz radiation, a decrease in transmitted terahertz amplitude upon photoexcitation corresponds to an increase in conductivity, σ, in the sample, which is proportional to the product of mobility, μ, and carrier density, N.

$$\Delta\mathrm{THz} \propto \Delta\sigma \propto \Delta(N\mu) \quad (1)$$

Using this relationship, measurement of the broadband terahertz response (peak time domain value) to photoexcitation provides a relatively straightforward method for determining the rate and efficiency of electron injection. To illustrate this point, a representative TRTS trace for TiO_2 nanoparticles sensitized with the ruthenium-polypyridyl sensitizer N719 (N719 = *cis*-diisothiocyanato-bis(2,2′-bipyridyl-4,4′-

DOI: 10.1021/ar500363q
Acc. Chem. Res. 2015, 48, 1423−1431

dicarboxylato)ruthenium(II) bis(tetrabutylammonium)) is shown in Figure 2. The sensitizer is photoexcited at 400 nm,

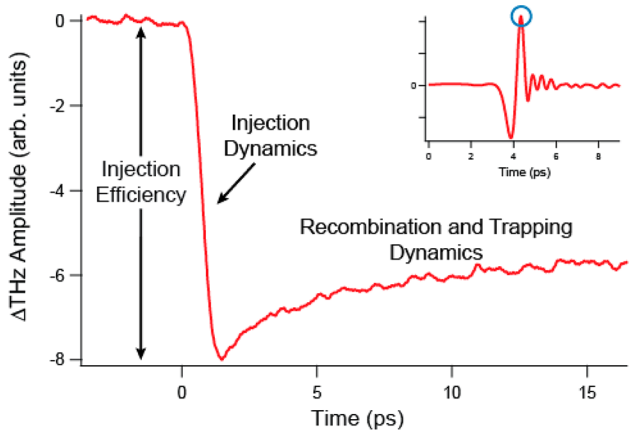

Figure 2. A representative TRTS measurement for a thin film of Degussa P25 TiO_2 nanoparticles (~21 nm diameter, 70% anatase, 30% rutile) sensitized with N719 and photoexcited at 400 nm. Time zero is defined as the time when the pump and probe pulses are temporally overlapped in the sample, and positive times correspond to situations where the pump pulse arrives at the sample prior to the terahertz probe pulse. The inset displays a time-domain trace of the terahertz probe pulse. Only the peak amplitude is monitored, as indicated by the small, blue circle.

a wavelength where N719 absorbs strongly but TiO_2 does not. The change in peak terahertz amplitude is then measured as a function of the time delay between the optical pump and terahertz probe pulses to determine the change in conductivity versus time.

For bare TiO_2, the 400 nm pump light is below the band gap, and no change in terahertz amplitude is observed following excitation. When the dye is present, electrons are injected into the TiO_2 conduction band following photoexcitation, and the terahertz amplitude decreases in proportion to the change in conductivity of the semiconductor. If mobility is held constant (as when we compare several different sensitizers on identical, uniform TiO_2 nanoparticle films), then the change in terahertz amplitude is dependent on the carrier density alone and is proportional to the relative efficiency of electron injection. In addition to the electron injection efficiency, the dynamics of injection and trapping (or recombination) can be determined as indicated in Figure 2. For N719 on TiO_2, the electron injection time scale is faster than the 300−400 fs response time of the instrument, and the signal recovery, which occurs on a roughly 50 ps time scale, most likely corresponds to trapping as opposed to recombination.[23] For a more detailed description of the experimental apparatus, see ref 22.

In addition to the time-domain analysis shown in Figure 2, terahertz spectroscopy can also be used to determine the far-infrared complex-valued frequency-dependent photoconductivity as a function of pump−probe delay time, giving insight into the mechanism of conductivity and charge transport. Because a discussion of these experiments is beyond the scope of this Account, the reader is referred to refs 8, 18−20, and 24 for more information.

HIGH-POTENTIAL PORPHYRINS

Porphyrins, which are the primary light-harvesting pigments used in photosynthesis, have been widely investigated for use in DSSCs due to their strong visible absorbance and synthetic tunability and have been incorporated into some of the highest efficiency DSSCs to date.[7] A series of free-base and metalated bis- and tris-pentafluorophenyl porphyrins (Figure 3) were thus investigated for use in a water oxidation device.

One attractive feature of porphyrins is that their photophysical and electrochemical properties can be easily tuned with minor structural changes. Porphyrins have two main sets of features in the visible region of the spectrum: the *Q*-band (500−600 nm, $\varepsilon = 10^3$−10^4 M^{-1} cm^{-1}), which corresponds to excitations from the ground state (S_0) to the first singlet excited states (S_1), and the Soret or *B* band (~400 nm, $\varepsilon = 10^5$ M^{-1} cm^{-1}), which corresponds to excitations from the porphyrin ground state to its second singlet excited state (S_2). Changes to the porphyrin ring substituents and to the central substituent can dramatically alter these bands.[25]

More importantly for optimizing porphyrins for water oxidation, absolute energy levels (reduction potentials) also change with fluorination and metalation. Addition of perfluorophenyl groups to the meso positions increases the reduction potential (lowers the Gibbs free energy) due to destabilization of the radical cation species.[26,27] The reduction potential is increased by roughly 100 mV for each pentafluorophenyl ring in the series $H_2P \rightarrow H_2PF_5 \rightarrow H_2PF_{10} \rightarrow H_2PF_{15}$. As a result, the potential is better positioned for water oxidation, as seen when we compare H_2TPP and H_2PF_{15} in Figure 4. Metalation further alters both the reduction potential and energy difference between ground and excited states, as shown in Figure 4 for Zn^{2+}, Ni^{2+}, Cu^{2+}, and Pd^{2+}.

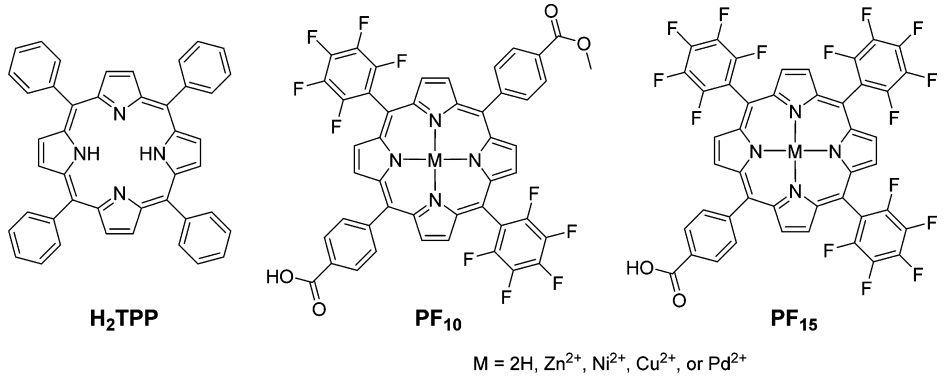

Figure 3. Structures of the porphyrins used in this study. H_2TPP = tetraphenylporphyrin, PF_{10} = 5-(4-carbomethoxyphenyl)-15-(4-carboxyphenyl)-10,20-bis(pentafluorophenyl)porphyrin, and PF_{15} = 5-(4-carboxyphenyl)-10,15,20-tris(pentafluorophenyl)porphyrin.

DOI: 10.1021/ar500363q
Acc. Chem. Res. 2015, 48, 1423−1431

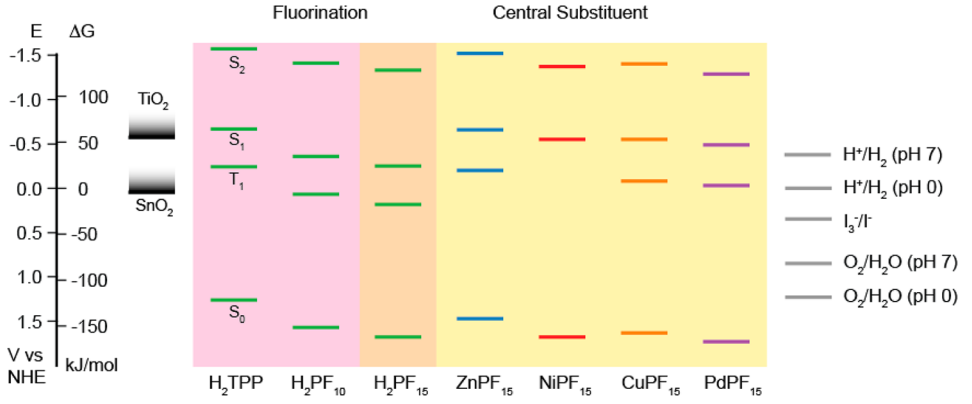

Figure 4. Effect of fluorination and metalation on the reduction potential of the ground (S_0) and excited states (S_2, S_1, and T_1) of various free-base and metalated porphyrins. The potentials for water oxidation and hydrogen reduction and the band edges of TiO_2 and SnO_2 (at pH 7) are also included.

ELECTRON INJECTION INTO TiO_2

Electron injection efficiencies for free-base and metalated versions of PF_{15} bound to TiO_2 nanoparticles were limited by the positioning of the excited states relative to the TiO_2 conduction band edge. As shown in the TRTS measurements in Figure 5A, only $ZnPF_{15}$ displays significant electron injection. This result can be understood by considering the position of the porphyrin excited states relative to the TiO_2 band edge (Figure 4) and the lifetimes of the various excited states. While all of the S_2 states are higher in energy than the band edge, the only S_1 state above the band edge and able to inject is that of $ZnPF_{15}$. Furthermore, the S_2 states of Cu^{2+}, Pd^{2+}, Ni^{2+}, and free-base porphyrins have sub-picosecond lifetimes,[28,29] whereas the S_2 states of Zn porphyrins can live as long as 2 ps.[30] As a result, only $ZnPF_{15}$ displays significant electron injection, although arguments can be made for $CuPF_{15}$ and H_2PF_{15} (see ref 10 for a more complete discussion).

Similar results were observed for the Zn^{2+}, Pd^{2+}, and free-base versions of PF_{10}.[11] Although the potentials are shifted to higher energies (lower potentials) by approximately 100 meV compared with the analogous PF_{15} compounds, the energy landscape remains the same, and only $ZnPF_{10}$ displays measurable electron injection into TiO_2.

These results highlight the difficulty with designing sensitizers compatible with water splitting for use with TiO_2 and indicate that TiO_2 may not be a suitable photoanode choice for water splitting. With the high potentials required for water oxidation, the sensitizer excited states lie too close to the band edge, or even below it, to provide efficient electron injection. Furthermore, these systems cannot be tuned to longer wavelengths in order to utilize a greater percentage of the solar spectrum, and they cannot take advantage of injection from longer-lived triplet states, which has been shown to increase injection efficiency.[31]

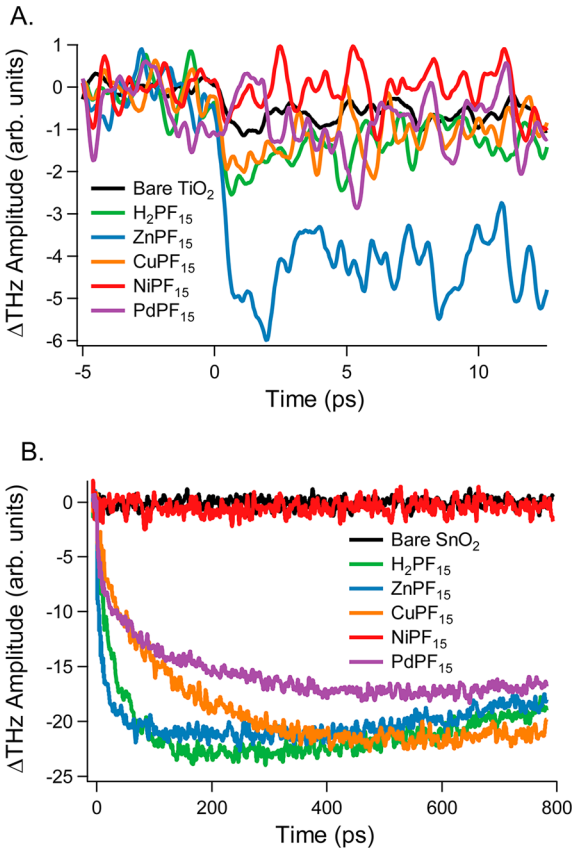

Figure 5. TRTS measurements of the electron injection from the PF_{15} porphyrins photoexcited at 400 nm into TiO_2 (A) and SnO_2 (B) nanoparticles. For bare TiO_2 or SnO_2, the 400 nm pump light is below the band gap, and no change in terahertz amplitude is observed following excitation (black lines).

ELECTRON INJECTION INTO SnO_2

The reduction potential of the SnO_2 band edge is ~0.5 V more positive than that of TiO_2, allowing for the possibility of electron injection from all of the S_1 and S_2 states and most of the T_1 states of the PF_{10} and PF_{15} porphyrins (Figure 4). Furthermore, electron injection is much slower for SnO_2 due to a decrease in the conduction band density of states.[21,32] With SnO_2, the rates of injection depend strongly on the lifetimes of the various excited states accessible following Soret band excitation, and these lifetimes are governed by the identity of the central substituent.

Electron injection from the PF_{15} sensitizers to SnO_2 following 400 nm excitation is shown in Figure 5B, and parameters obtained by fitting eq 2 to the injection dynamics for the PF_{15} and PF_{10} sensitizers are listed in Table 1.

$$\Delta THz = \Delta THz_0[A_1(e^{-t/\tau_1} - 1) + A_2(e^{-t/\tau_2} - 1) + (1 - e^{-t/\tau_r})] \quad (2)$$

DOI: 10.1021/ar500363q
Acc. Chem. Res. 2015, 48, 1423−1431

Table 1. Comparison of Electron Injection Dynamics and Efficiency of Free-Base and Metalated PF_{10} and PF_{15} Porphyrins

		faster injection				slower injection				
porphyrin	ΔTHz_0 (arb. units)	A_1	τ_1 (ps)	state	E^a	A_2	τ_2 (ps)	state	E^a	ref
H_2PF_{10}	16	0.39	2.08	S_2	−1.41	0.61	43.3	S_1	−0.36	11, 33
H_2PF_{15}	24	0.19	1.20	S_2	−1.33	0.81	37.4	S_1	−0.25	10
$ZnPF_{10}$	8.8	0.77	0.71	S_2		0.23	6.83	S_1	−0.77	11, 33
$ZnPF_{15}$	23	0.38	0.44	S_2	−1.52	0.62	18.1	S_1	−0.66	10
$PdPF_{10}$	15	0.51	2.85	S_1	−0.58	0.49	139	T_1	−0.12	11, 33
$PdPF_{15}$	21	0.44	5.14	S_1	−0.49	0.56	197	T_1	−0.03	10
$CuPF_{15}$	26	0.30	10.5	$^2S_1$	−0.55	0.70	180	$^2T_1$	−0.08	10

[a]Reported in V vs NHE.

The measured change in terahertz amplitude as a function of pump/probe delay time, ΔTHz, is modeled with a double exponential with time constants τ_1 and τ_2 and relative amplitudes A_1 and A_2 (where $A_1 + A_2 = 1$) to account for electron injection. A single exponential with time constant τ_r accounts for trapping or recombination, and ΔTHz_0 is a scaling factor that indicates the relative injection efficiency.

Among the PF_{15} porphyrins, the injection rates for $ZnPF_{15}$ and free-base PF_{15} were 5−10 times faster than those for $CuPF_{15}$ and $PdPF_{15}$, and $NiPF_{15}$ did not inject. The same general trends resulting from changes in the central substituent observed for PF_{15} were also seen for PF_{10}. Electron injection was fastest for $ZnPF_{10}$ ($\tau_1 = 0.71$ and $\tau_2 = 6.83$) and slowest for $PdPF_{10}$ ($\tau_1 = 2.85$ and $\tau_2 = 139$).

These results can be understood considering the competition between electron injection and deactivation of the porphyrin excited states, as the time scale of electron injection (sub-picosecond to hundreds of picoseconds) overlaps with the range of excited state lifetimes (sub-picosecond to micro-second). All of the porphyrins were excited to the S_2 state using 400 nm excitation, allowing for the possibility of relaxation to the lower-lying S_1 and T_1 states. The associated rates and efficiencies of internal conversion and intersystem crossing, and thus the lifetime of the excited states, strongly depend on the identity of the central substituent. Gouterman's classification of porphyrin emission as either fluorescent, phosphorescent, luminescent, or radiationless provides a useful framework for understanding the electron injection,[34] and a summary of the electron injection processes for all of the high potential porphyrins is provided in Figure 6.

Free-base and zinc porphyrins are fluorescent and thus display high quantum yields of emission from S_1. Additionally, they have fairly long-lived S_2 states (up to 2 ps for zinc porphyrins) and nanosecond S_1 state lifetimes.[27,34] The faster electron injection component for the zinc and free-base porphyrins, which is a picosecond or less in duration, must therefore correspond to injection from S_2. Because the slower component is well within the S_1 lifetime, it thus corresponds to injection from S_1. Whereas τ_2 is truly a measure of the injection time scale from S_1, τ_1 is simply the S_2 lifetime.

Pd^{2+} porphyrins are typically phosphorescent, and Cu^{2+} porphyrins are luminescent. Although their emission properties are slightly different, they give rise to very similar electron injection time scales and mechanisms. When Pd^{2+} is present, the lifetimes of the S_2 and S_1 states are decreased and intersystem crossing to T_1 is favored as a result of increased spin−orbit coupling and the heavy atom effect. Cu^{2+} has a similar effect, although the decreased lifetimes are due to paramagnetism, which causes increased mixing between excited states. As a result, the excited states can no longer be classified as either singlets or triplets and are denoted singdoublets (^2S) and tripdoublets (^2T), respectively. $PdPF_{15}$ and $CuPF_{15}$ both have short-lived S_2 states that relax before electron injection can occur. The fast component, τ_1, corresponds to injection from the S_1 ($PdPF_{15}$) or $^2S_1$ ($CuPF_{15}$) states that have lifetimes ranging from 13 to 20 ps,[25] and τ_2 corresponds to injection from T_1 ($PdPF_{15}$) or $^2T_1$ ($CuPF_{15}$) states with lifetimes on the order of nanoseconds to microseconds.[25,35] Analogous to the zinc and free-base porphyrins, τ_2 truly is a measure of the injection time scale from T_1, and τ_1 is simply the S_1 lifetime.

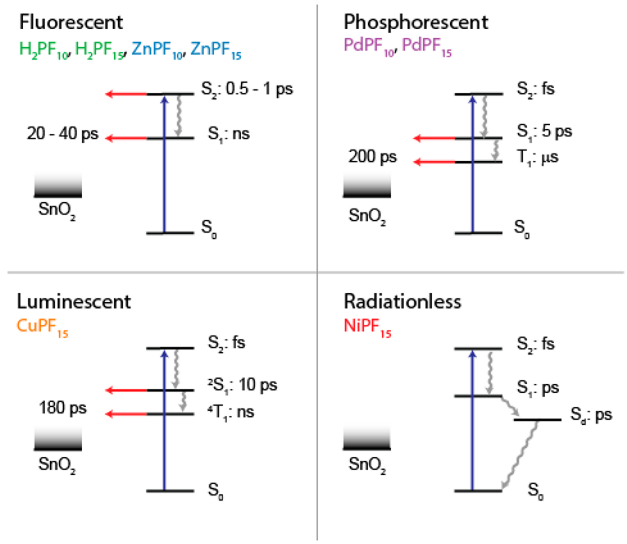

Figure 6. Summary of the electron injection and excited state deactivation for the PF_{10} and PF_{15} porphyrins bound to SnO_2 nanoparticles and excited at 400 nm.

The photophysics of Ni^{2+} porphyrins is dramatically different due to the presence of empty d orbitals on the nickel cation. The S_2 and S_1 states are both very short-lived and relax to metal-centered d states,[29] which in turn lack electronic coupling to the metal oxide surface, disfavoring injection even further.

CORRELATING TERAHERTZ RESULTS WITH MACROSCOPIC PERFORMANCE

It is instructive to compare results of terahertz measurements, which probe ∼10 nm length scales and sub-nanosecond timescales, with macroscopic device efficiencies. As stated in the Introduction, water oxidation devices currently have low efficiencies and lack a standard design. Therefore, DSSCs are often used to emulate device performance because they are more standardized and better understood. As such, DSSCs

DOI: 10.1021/ar500363q
Acc. Chem. Res. 2015, 48, 1423−1431

were fabricated using the PF_{10} porphyrins and SnO_2 nanoparticles (Table 2).

Table 2. Photovoltaic Parameters Measured at 100 mW/cm^2 Illumination for DSSCs Containing SnO_2 Photoanodes Sensitized with the PF_{10} Chromophores

dye	electrolyte	J (mA/cm^2)	V_{oc} (V)	FF	η (%)
H_2PF_{10}	I_3^-/I^-	1.01	0.31	0.32	0.10
	Br_3^-/Br^-	2.53	0.64	0.47	0.76
$ZnPF_{10}$	I_3^-/I^-	2.51	0.37	0.41	0.39
	Br_3^-/Br^-	1.32	0.59	0.51	0.40
$PdPF_{10}$	I_3^-/I^-	0.81	0.31	0.37	0.09
	Br_3^-/Br^-	3.37	0.66	0.45	1.00

Due to the high reduction potentials of the porphyrin sensitizers, the Br^-/Br_3^- redox couple was used instead of I^-/I_3^- since its reduction potential is ~500 mV more positive than I^-/I_3^-. The Br^-/Br_3^- cells were found to have larger open circuit voltage (V_{oc}) values and efficiencies (η) than their I^-/I_3^- counterparts because potential losses due to dye regeneration were minimized.[11,36] The ranking of DSSC efficiencies using the Br^-/Br_3^- couple ($PdPF_{10}$ > H_2PF_{10} > $ZnPF_{10}$) loosely correlates with the values of the injection time scale and with ΔTHz_0, but not the driving force for electron injection (see Tables 1 and 2). These results suggest that the kinetics of electron injection in these particular systems are more important than the energetics (i.e., the molecular excited state energy relative to the conduction band minimum) in determining the efficiency. Furthermore, slower injection leads to increased overall cell efficiency, presumably because it results in a larger overall injection yield. Durrant and coworkers have observed similar kinetic effects in DSSCs and have described the importance of balancing the various physical processes in order to prevent competition with unwanted processes.[37]

WATER STABLE ANCHORING GROUPS

The anchoring group is essential for efficient electron injection because it establishes the electronic coupling between the sensitizer and the metal oxide. In DSSCs, carboxylate is the most popular anchoring group due to its ease of synthesis and relative stability under the operating conditions of the cell.[2] Carboxylate-anchored sensitizers, however, have been shown to desorb from TiO_2 over a wide pH range when immersed in water.[38] For water oxidation, several water-stable alternatives have been identified including phosphonic acid,[39,40] hydroxamic acid,[38,41−43] acetylacetone (acac),[9,44] boronic acid,[45] silanes,[46] and catechol.[47]

In order to test the relative injection efficiencies of several anchoring groups, a modular assembly technique, which has shown success in DSSCs,[48−50] was used. The semiconductor surface is first sensitized with a small linker molecule (L), which contains an anchoring group (A) to bind to the semiconductor, and a Lewis base such as a pyridyl nitrogen to coordinate with a chromophore (Figure 7A). Zinc porphyrins are a popular choice because of their ability to axially bind ligands.[51] Accordingly, the $ZnPF_{10}$ diester was chosen to provide relevance to water oxidation and to eliminate the possibility of direct binding of the porphyrin to the TiO_2 surface. This allowed several anchoring groups (Figure 7B) to be screened with minimal synthetic challenge. In addition, the modular assembly approach decouples the porphyrin from the linker molecule, allowing for comparisons between anchoring groups that are less influenced by interactions with the chromophore.[14]

TRTS measurements for all of the $ZnPF_{10}$−linker assemblies are shown in Figure 8A. Although all of the injection time scales are faster than the instrument response time, variations in injection efficiency are apparent. Compared with the carboxylate assembly, the phosphonate, acac, and borate versions all exhibited less efficient electron injection. The hydroxamate, however, injected as efficiently as or even more efficiently than the carboxylate.

To help explain these differences in electron injection efficiencies, the conductance, G, of each linker molecule was calculated using nonequilibrium Green's functions and the semiempirical extended-Hückel Hamiltonian.[14] A kinetic model was then fit to the terahertz data in Figure 8A[14] in order to determine a value of maximum electron injection, X_0, which corresponds roughly to the magnitude of the maximum observed change in terahertz amplitude. A plot of X_0 against the calculated conductance yielded a linear correlation (Figure 8B), suggesting that the conductance of the different linkers has a direct effect on the electron injection efficiency.

Understanding why conductivity depends on anchoring group requires analysis of frontier molecular orbitals and

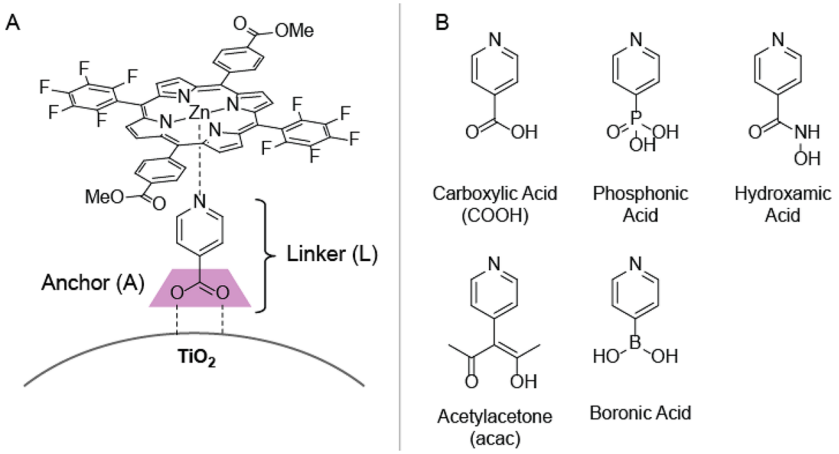

Figure 7. (A) Modular assembly of the $ZnPF_{10}$ diester on the TiO_2 surface via a pyridyl linker molecule (L) containing a carboxylate anchoring group (A). (B) Five 4-pyridyl linker molecules functionalized with various anchoring groups for binding to the TiO_2 surface.

DOI: 10.1021/ar500363q
Acc. Chem. Res. 2015, 48, 1423−1431

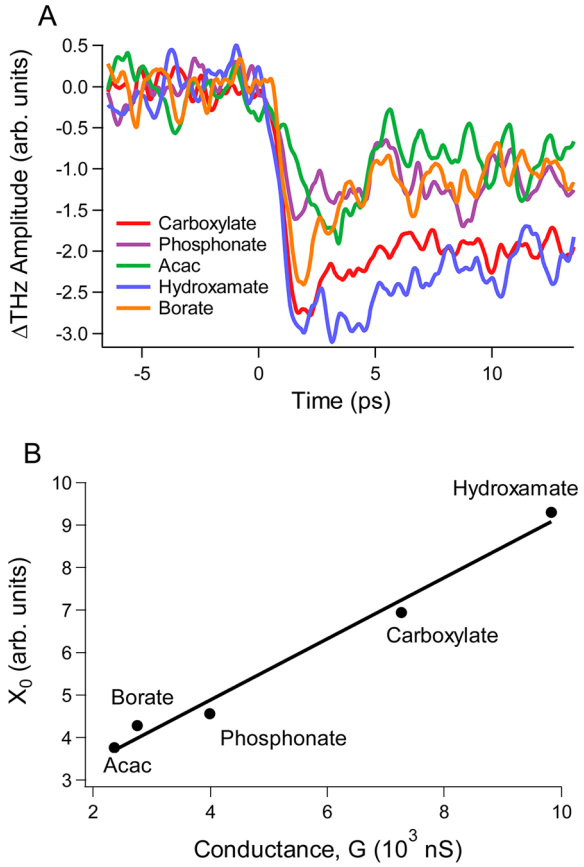

Figure 8. (A) TRTS measurements comparing the electron injection efficiency into TiO_2 of the $ZnPF_{10}$-diester modular assemblies with pyridyl linker molecules containing different anchoring groups. (B) Change in terahertz amplitude (X_0) at the time of maximum attenuation vs conductance (G) computed for the various linkers.

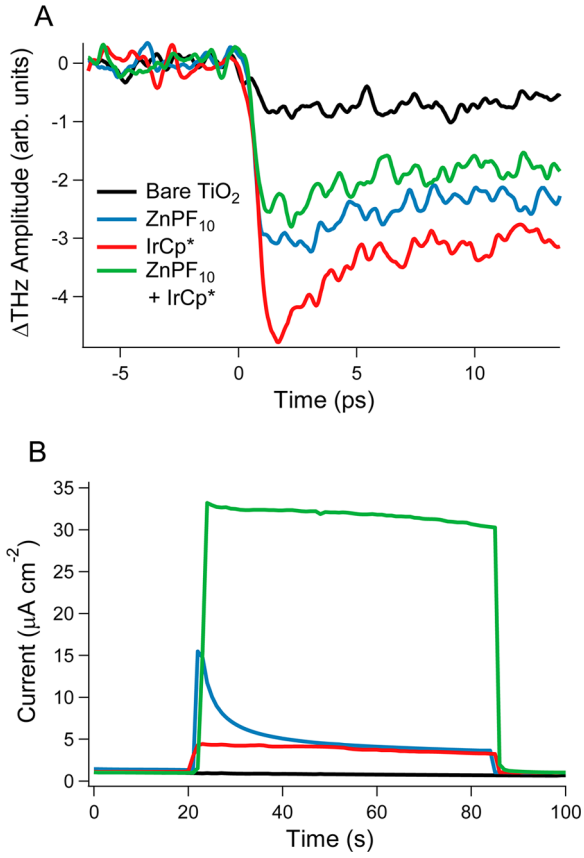

Figure 9. (A) TRTS measurements of the electron injection following 400 nm excitation for thin films of TiO_2 nanoparticles sensitized with $ZnPF_{10}$ alone, IrCp* alone, and $ZnPF_{10}$ plus IrCp*.[12] (B) Photocurrent measured for the same photoanodes.[12] Reproduced from ref 12 by permission of The Royal Society of Chemistry.

surface binding structures. The conductance for 4-pyridyl-acac is lowest because its lowest unoccupied molecular orbital (LUMO) is centered on the acac moiety and is not conjugated with the pyridine and delocalized over the entire molecule as for the other linkers.[14] Similarly, the conductance of 4-pyridyl-phosphonate and 4-pyridyl-borate is limited by the presence of the heteroatom, which inhibits electron tunneling through the linker. The differences between the carboxylate and hydroxamate conductances are more difficult to rationalize. One possible explanation could involve differences in surface binding, although the exact binding modes are currently not well understood.

CATALYST INCORPORATION

One of the next challenges facing photoelectrochemical water oxidation is determining the best method for incorporating the catalyst. Early examples of catalyst-containing dye-sensitized photoanodes highlight the difficulty of incorporating the catalyst and maintaining the performance of other components of the system.[5,6] In the first attempt from the Yale solar collaboration, TiO_2 was cosensitized with $ZnPF_{10}$ and an IrCp* precatalyst[52] modified with a carboxylate anchoring group.[12] Although electrochemical measurements demonstrated increased photocurrent with cosensitization, TRTS measurements revealed that the electron injection efficiency decreased (Figure 9), most likely due to quenching of the porphyrin excited state by the iridium species. This example demonstrates that the incorporation of the catalyst will require significant tuning of the physical and chemical properties of all species involved. Furthermore, it emphasizes the need for studying electron injection in fully functioning cells so that better comparisons can be made with other experimental techniques and so that the role of electron injection in device performance can be determined.

CONCLUSION AND OUTLOOK

Global energy needs are immense, and one avenue worth pursuing is artificial photosynthesis. This strategy requires efficient catalysts for water oxidation as well as a means to photoactivate them and transport the electrons required to make fuels. We have shown that fluorinated and metalated porphyrins are an excellent choice for the light-harvesting chromophore because their energy levels and redox potentials are compatible with water oxidation, they are oxidation-resistant, and they can be bound to metal oxide surfaces even in the presence of water when appropriate anchoring groups are used.

Future work will bring together the anchor, linker/chromophore, and water oxidation catalyst as a single entity. This will allow efficient water oxidation as part of a larger scheme for solar fuel generation. Ultrafast processes are crucial to highly efficient solar cells in much the same way that they are crucial for the primary charge separation event in natural photosynthesis. The only way to fully understand and exploit

DOI: 10.1021/ar500363q
Acc. Chem. Res. 2015, 48, 1423−1431

them is by making measurements on a sub-picosecond timescale.

AUTHOR INFORMATION

Corresponding Author

*E-mail: charles.schmuttenmaer@yale.edu.

Present Address

[†]Department of Physics, University of Oxford, Clarendon Laboratory, Parks Road, Oxford OX1 3PU, U.K.

Funding

This work was funded by the U.S. Department of Energy Office of Science, Office of Basic Energy Sciences, under Award Number DE-FG02-07ER15909.

Notes

The authors declare no competing financial interest.

Biographies

Rebecca L. Milot received her B.S. in Chemistry from Providence College in 2007 and Ph.D. from Yale University in 2014. She is currently a postdoctoral research associate at the University of Oxford.

Charles A. Schmuttenmaer received his B.S. degree in Chemistry from the University of Illinois in 1985 and his Ph.D. from University of California, Berkeley, in 1991. He was a postdoctoral associate at the University of Rochester until 1994 and then began his independent career at Yale University where he has been ever since. His primary research interests encompass all things terahertz.

REFERENCES

(1) O'Regan, B.; Grätzel, M. A Low-Cost, High-Efficiency Solar-Cell Based on Dye-Sensitized Colloidal TiO_2 Films. *Nature* **1991**, *353*, 737−740.

(2) Hagfeldt, A.; Boschloo, G.; Sun, L. C.; Kloo, L.; Pettersson, H. Dye-Sensitized Solar Cells. *Chem. Rev.* **2010**, *110*, 6595−6663.

(3) Kousksou, T.; Bruel, P.; Jamil, A.; El Rhafiki, T.; Zeraouli, Y. Energy Storage: Applications and Challenges. *Sol. Energy Mater. Sol. Cells* **2014**, *120*, 59−80.

(4) McConnell, I.; Li, G. H.; Brudvig, G. W. Energy Conversion in Natural and Artificial Photosynthesis. *Chem. Biol.* **2010**, *17*, 434−447.

(5) Young, K. J.; Martini, L. A.; Milot, R. L.; Snoeberger, R. C., III; Batista, V. S.; Schmuttenmaer, C. A.; Crabtree, R. H.; Brudvig, G. W. Light-Driven Water Oxidation for Solar Fuels. *Coord. Chem. Rev.* **2012**, *256*, 2503−2520.

(6) Swierk, J. R.; Mallouk, T. E. Design and Development of Photoanodes for Water-Splitting Dye-Sensitized Photoelectrochemical Cells. *Chem. Soc. Rev.* **2013**, *42*, 2357−2387.

(7) Duan, L. L.; Tong, L. P.; Xu, Y. H.; Sun, L. C. Visible Light-Driven Water Oxidation-From Molecular Catalysts to Photoelectrochemical Cells. *Energy Environ. Sci.* **2011**, *4*, 3296−3313.

(8) Baxter, J. B.; Richter, C.; Schmuttenmaer, C. A. Ultrafast Carrier Dynamics in Nanostructures for Solar Fuels. *Annu. Rev. Phys. Chem.* **2014**, *65*, 423−447.

(9) McNamara, W. R.; Snoeberger, R. C.; Li, G.; Schleicher, J. M.; Cady, C. W.; Poyatos, M.; Schmuttenmaer, C. A.; Crabtree, R. H.; Brudvig, G. W.; Batista, V. S. Acetylacetonate Anchors for Robust Functionalization of TiO_2 Nanoparticles with Mn(II)-Terpyridine Complexes. *J. Am. Chem. Soc.* **2008**, *130*, 14329−14338.

(10) Milot, R. L.; Moore, G. F.; Crabtree, R. H.; Brudvig, G. W.; Schmuttenmaer, C. A. Electron Injection Dynamics from Photoexcited Porphyrin Dyes into SnO_2 and TiO_2 Nanoparticles. *J. Phys. Chem. C* **2013**, *117*, 21662−21670.

(11) Moore, G. F.; Konezny, S. J.; Song, H. E.; Milot, R. L.; Blakemore, J. D.; Lee, M. L.; Batista, V. S.; Schmuttenmaer, C. A.; Crabtree, R. H.; Brudvig, G. W. Bioinspired High-Potential Porphyrin Photoanodes. *J. Phys. Chem. C* **2012**, *116*, 4892−4902.

(12) Moore, G. F.; Blakemore, J. D.; Milot, R. L.; Hull, J. F.; Song, H. E.; Cai, L.; Schmuttenmaer, C. A.; Crabtree, R. H.; Brudvig, G. W. A Visible Light Water-Splitting Cell with a Photoanode Formed by Codeposition of a High-Potential Porphyrin and an Iridium Water-Oxidation Catalyst. *Energy Environ. Sci.* **2011**, *4*, 2389−2392.

(13) Martini, L. A.; Moore, G. F.; Milot, R. L.; Cai, L. Z.; Sheehan, S. W.; Schmuttenmaer, C. A.; Brudvig, G. W.; Crabtree, R. H. Modular Assembly of High-Potential Zinc Porphyrin Photosensitizers Attached to TiO_2 with a Series of Anchoring Groups. *J. Phys. Chem. C* **2013**, *117*, 14526−14533.

(14) Negre, C. F. A.; Milot, R. L.; Martini, L. A.; Ding, W.; Crabtree, R. H.; Schmuttenmaer, C. A.; Batista, V. S. Efficiency of Interfacial Electron Transfer from Zn-Porphyrin Dyes into TiO_2 Correlated to the Linker Single Molecule Conductance. *J. Phys. Chem. C* **2013**, *117*, 24462−24470.

(15) Williams, M. R. C.; Aschaffenburg, D. J.; Ofori-Okai, B. K.; Schmuttenmaer, C. A. Intermolecular Vibrations in Hydrophobic Amino Acid Crystals: Experiments and Calculations. *J. Phys. Chem. B* **2013**, *117*, 10444−10461.

(16) Markelz, A. G. Terahertz Dielectric Sensitivity to Biomolecular Structure and Function. *IEEE J. Sel. Top. Quantum Electron.* **2008**, *14*, 180−190.

(17) Beard, M. C.; Turner, G. M.; Schmuttenmaer, C. A. Terahertz Spectroscopy. *J. Phys. Chem. B* **2002**, *106*, 7146−7159.

(18) Schmuttenmaer, C. A. Exploring Dynamics in the Far-Infrared with Terahertz Spectroscopy. *Chem. Rev.* **2004**, *104*, 1759−1779.

(19) Němec, H.; Kužel, P.; Sundström, V. Charge Transport in Nanostructured Materials for Solar Energy Conversion Studied by Time-Resolved Terahertz Spectroscopy. *J. Photochem. Photobiol., A* **2010**, *215*, 123−139.

(20) Turner, G. M.; Beard, M. C.; Schmuttenmaer, C. A. Carrier Localization and Cooling in Dye-Sensitized Nanocrystalline Titanium Dioxide. *J. Phys. Chem. B* **2002**, *106*, 11716−11719.

(21) Tiwana, P.; Docampo, P.; Johnston, M. B.; Snaith, H. J.; Herz, L. M. Electron Mobility and Injection Dynamics in Mesoporous ZnO, SnO_2, and TiO_2 Films Used in Dye-Sensitized Solar Cells. *ACS Nano* **2011**, *5*, 5158−5166.

(22) Beard, M. C.; Turner, G. M.; Schmuttenmaer, C. A. Subpicosecond Carrier Dynamics in Low-Temperature Grown GaAs as Measured by Time-Resolved Terahertz Spectroscopy. *J. Appl. Phys.* **2001**, *90*, 5915−5923.

(23) Ardo, S.; Meyer, G. J. Photodriven Heterogeneous Charge Transfer with Transition-Metal Compounds Anchored to TiO_2 Semiconductor Surfaces. *Chem. Soc. Rev.* **2009**, *38*, 115−164.

(24) Lloyd-Hughes, J.; Jeon, T. I. A Review of the Terahertz Conductivity of Bulk and Nano-Materials. *J. Infrared, Millimeter, Terahertz Waves* **2012**, *33*, 871−925.

(25) Kalyanasundaram, K. *Photochemistry of Polypyridine and Porphyrin Complexes*; Acedemic Press: New York, 1992.

(26) Hodge, J. A.; Hill, M. G.; Gray, H. B. Electrochemistry of Nonplanar Zinc(II) Tetrakis(Pentafluorophenyl)porphyrins. *Inorg. Chem.* **1995**, *34*, 809−812.

(27) Yang, S. I.; Seth, J.; Strachan, J. P.; Gentemann, S.; Kim, D.; Holten, D.; Lindsey, J. S.; Bocian, D. F. Ground and Excited State Electronic Properties of Halogenated Tetraarylporphyrins. Tuning the Building Blocks for Porphyrin-Based Photonic Devices. *J. Porphyrins Phthalocyanines* **1999**, *3*, 117−147.

(28) Yeon, K. Y.; Jeong, D.; Kim, S. K. Intrinsic Lifetimes of the Soret Bands of the Free-Base Tetraphenylporphine (H_2TPP) and Cu(II)-TPP in the Condensed Phase. *Chem. Commun.* **2010**, *46*, 5572−5574.

(29) Rodriguez, J.; Holten, D. Ultrafast Vibrational Dynamics of a Photoexcited Metalloporphyrin. *J. Chem. Phys.* **1989**, *91*, 3525−3531.

(30) Liu, X.; Yeow, E. K. L.; Velate, S.; Steer, R. P. Photophysics and Spectroscopy of the Higher Electronic States of Zinc Metalloporphyrins: A Theoretical and Experimental Study. *Phys. Chem. Chem. Phys.* **2006**, *8*, 1298−1309.

(31) Listorti, A.; Lopez-Duarte, I.; Martinez-Diaz, M. V.; Torres, T.; DosSantos, T.; Barnes, P. R. F.; Durrant, J. R. Zn(II) versus Ru(II) Phthalocyanine-Sensitised Solar Cells. A Comparison between Singlet

DOI: 10.1021/ar500363q
Acc. Chem. Res. 2015, 48, 1423−1431

and Triplet Electron Injectors. *Energy Environ. Sci.* **2010**, *3*, 1573−1579.
(32) Ai, X.; Anderson, N. A.; Guo, J. C.; Lian, T. Q. Electron Injection Dynamics of Ru Polypyridyl Complexes on SnO_2 Nanocrystalline Thin Films. *J. Phys. Chem. B* **2005**, *109*, 7088−7094.
(33) Milot, R. L. Interfacial Electron Transfer and Transient Photoconductivity Studied with Terahertz Spectroscopy. Ph.D. Thesis, Yale University, 2014.
(34) Gouterman, M.: Optical Spectra and Electronic Structure of Porphyrins. In *The Porphyrins*; Dolphin, D., Ed.; Academic Press: New York, 1978; Vol. *III*.
(35) Cunningham, K. L.; McNett, K. M.; Pierce, R. A.; Davis, K. A.; Harris, H. H.; Falck, D. M.; McMillin, D. R. EPR Spectra, Luminescence Data, and Radiationless Decay Processes of Copper(II) Porphyrins. *Inorg. Chem.* **1997**, *36*, 608−613.
(36) Boschloo, G.; Hagfeldt, A. Characteristics of the Iodide/Triiodide Redox Mediator in Dye-Sensitized Solar Cells. *Acc. Chem. Res.* **2009**, *42*, 1819−1826.
(37) Haque, S. A.; Palomares, E.; Cho, B. M.; Green, A. N. M.; Hirata, N.; Klug, D. R.; Durrant, J. R. Charge Separation versus Recombination in Dye-Sensitized Nanocrystalline Solar Cells: The Minimization of Kinetic Redundancy. *J. Am. Chem. Soc.* **2005**, *127*, 3456−3462.
(38) McNamara, W. R.; Snoeberger, R. C.; Li, G. H.; Richter, C.; Allen, L. J.; Milot, R. L.; Schmuttenmaer, C. A.; Crabtree, R. H.; Brudvig, G. W.; Batista, V. S. Hydroxamate Anchors for Water-Stable Attachment to TiO_2 Nanoparticles. *Energy Environ. Sci.* **2009**, *2*, 1173−1175.
(39) Pechy, P.; Rotzinger, F. P.; Nazeeruddin, M. K.; Kohle, O.; Zakeeruddin, S. M.; Humphrybaker, R.; Grätzel, M. Preparation of Phosphonated Polypyridyl Ligands to Anchor Transition-Metal Complexes on Oxide Surfaces - Application for the Conversion of Light to Electricity with Nanocrystalline TiO_2 Films. *J. Chem. Soc., Chem. Commun.* **1995**, 65−66.
(40) Park, H.; Bae, E.; Lee, J. J.; Park, J.; Choi, W. Effect of the Anchoring Group in Ru-bipyridyl Sensitizers on the Photoelectrochemical Behavior of Dye-Sensitized TiO_2 Electrodes: Carboxylate versus Phosphonate Linkages. *J. Phys. Chem. B* **2006**, *110*, 8740−8749.
(41) McNamara, W. R.; Milot, R. L.; Song, H. E.; Snoeberger, R. C.; Batista, V. S.; Schmuttenmaer, C. A.; Brudvig, G. W.; Crabtree, R. H. Water-Stable, Hydroxamate Anchors for Functionalization of TiO_2 Surfaces with Ultrafast Interfacial Electron Transfer. *Energy Environ. Sci.* **2010**, *3*, 917−923.
(42) Brewster, T. P.; Konezny, S. J.; Sheehan, S. W.; Martini, L. A.; Schmuttenmaer, C. A.; Batista, V. S.; Crabtree, R. H. Hydroxamate Anchors for Improved Photoconversion in Dye-Sensitized Solar Cells. *Inorg. Chem.* **2013**, *52*, 6752−6764.
(43) Koenigsmann, C.; Ripolles, T. S.; Brennan, B. J.; Negre, C. F. A.; Koepf, M.; Durrell, A. C.; Milot, R. L.; Torre, J. A.; Crabtree, R. H.; Batista, V. S.; Brudvig, G. W.; Bisquert, J.; Schmuttenmaer, C. A. Substitution of a Hydroxamic Acid Anchor into the MK-2 Dye for Enhanced Photovoltaic Performance and Water Stability in a DSSC. *Phys. Chem. Chem. Phys.* **2014**, *16*, 16629−16641.
(44) Heimer, T. A.; Darcangelis, S. T.; Farzad, F.; Stipkala, J. M.; Meyer, G. J. An Acetylacetonate-Based Semiconductor-Sensitizer Linkage. *Inorg. Chem.* **1996**, *35*, 5319−5324.
(45) Altobello, S.; Bignozzi, C. A.; Caramori, S.; Larramona, G.; Quici, S.; Marzanni, G.; Lakhmiri, R. Sensitization of TiO_2 with Ruthenium Complexes Containing Boronic Acid Functions. *J. Photochem. Photobiol., A* **2004**, *166*, 91−98.
(46) Brennan, B. J.; Portoles, M. J. L.; Liddell, P. A.; Moore, T. A.; Moore, A. L.; Gust, D. Comparison of Silatrane, Phosphonic Acid, and Carboxylic Acid Functional Groups for Attachment of Porphyrin Sensitizers to TiO_2 in Photoelectrochemical Cells. *Phys. Chem. Chem. Phys.* **2013**, *15*, 16605−16614.
(47) Abuabara, S. G.; Cady, C. W.; Baxter, J. B.; Schmuttenmaer, C. A.; Crabtree, R. H.; Brudvig, G. W.; Batista, V. S. Ultrafast Photooxidation of Mn(II)-Terpyridine Complexes Covalently Attached to TiO_2 Nanoparticles. *J. Phys. Chem. C* **2007**, *111*, 11982−11990.
(48) Subbaiyan, N. K.; Wijesinghe, C. A.; D'Souza, F. Supramolecular Solar Cells: Surface Modification of Nanocrytalline TiO_2 with Coordinating Ligands To Immobilize Sensitizers and Dyads via Metal−Ligand Coordination for Enhanced Photocurrent Generation. *J. Am. Chem. Soc.* **2009**, *131*, 14646−14647.
(49) Brumbach, M. T.; Boal, A. K.; Wheeler, D. R. Metalloporphyrin Assemblies on Pyridine-Functionalized Titanium Dioxide. *Langmuir* **2009**, *25*, 10685−10690.
(50) Nazeeruddin, M. K.; Humphry-Baker, R.; Grätzel, M.; Murrer, B. A. Efficient Near IR Sensitization of Nanocrystalline TiO_2 Films by Ruthenium Phthalocyanines. *Chem. Commun.* **1998**, 719−720.
(51) Nappa, M.; Valentine, J. S. Influence of Axial Ligands on Metalloporphyrin Visible Absorption Spectra - Complexes of Tetraphenylporphinatozinc. *J. Am. Chem. Soc.* **1978**, *100*, 5075−5080.
(52) Hintermair, U.; Sheehan, S. W.; Parent, A. R.; Ess, D. H.; Richens, D. T.; Vaccaro, P. H.; Brudvig, G. W.; Crabtree, R. H. Precursor Transformation during Molecular Oxidation Catalysis with Organometallic Iridium Complexes. *J. Am. Chem. Soc.* **2013**, *135*, 10837−10851.

DOI: 10.1021/ar500363q
Acc. Chem. Res. 2015, 48, 1423−1431